Monthly Notices of the ROYAL ASTRONOMICAL SOCIETY

MNRAS **496,** 3402–3411 (2020) doi:10.1093/mnras/staa1801
Advance Access publication 2020 June 20

A measurement of the Hubble constant from Type II supernovae

T. de Jaeger [1]★† B. E. Stahl [1,2]‡ W. Zheng,[1] A. V. Filippenko,[1,3]§ A. G. Riess[4,5] and L. Galbany [6]

[1]*Department of Astronomy, University of California, Berkeley, CA 94720, USA*
[2]*Department of Physics, University of California, Berkeley, CA 94720, USA*
[3]*Miller Institute for Basic Research in Science, University of California, Berkeley, CA 94720, USA*
[4]*Space Telescope Science Institute, Baltimore, MD 21218, USA*
[5]*Department of Physics & Astronomy, The Johns Hopkins University, Baltimore, MD 21218, USA*
[6]*Departamento de Física Teórica y del Cosmos, Universidad de Granada, E-18071 Granada, Spain*

Accepted 2020 June 18. Received 2020 June 17; in original form 2020 June 2

ABSTRACT

Progressive increases in the precision of the Hubble-constant measurement via Cepheid-calibrated Type Ia supernovae (SNe Ia) have shown a discrepancy of $\sim 4.4\sigma$ with the current value inferred from *Planck* satellite measurements of the cosmic microwave background radiation and the standard Λcold dark matter (ΛCDM) cosmological model. This disagreement does not appear to be due to known systematic errors and may therefore be hinting at new fundamental physics. Although all of the current techniques have their own merits, further improvement in constraining the Hubble constant requires the development of as many independent methods as possible. In this work, we use SNe II as standardisable candles to obtain an independent measurement of the Hubble constant. Using seven SNe II with host-galaxy distances measured from Cepheid variables or the tip of the red giant branch, we derive $H_0 = 75.8^{+5.2}_{-4.9}$ km s^{-1} Mpc^{-1} (statistical errors only). Our value favours that obtained from the conventional distance ladder (Cepheids + SNe Ia) and exhibits a difference of 8.4 km s^{-1} Mpc^{-1} from the *Planck* + ΛCDM value. Adding an estimate of the systematic errors (2.8 km s^{-1} Mpc^{-1}) changes the $\sim 1.7\sigma$ discrepancy with *Planck* +ΛCDM to $\sim 1.4\sigma$. Including the systematic errors and performing a bootstrap simulation, we confirm that the local H_0 value exceeds the value from the early Universe with a confidence level of 95 per cent. As in this work, we only exchange SNe II for SNe Ia to measure extragalactic distances, we demonstrate that there is no evidence that SNe Ia are the source of the H_0 tension.

Key words: supernovae: general – galaxies: distances and redshifts – distance scale.

1 INTRODUCTION

The current expansion rate of the Universe, known as the Hubble constant (H_0), remains one of the most important parameters in modern cosmology. Determining an accurate value is essential for obtaining information regarding our Universe, including its age and evolution. Since the discovery of the expansion of the Universe (Lemaître 1927; Hubble 1929), many efforts have been made to measure H_0 precisely and decrease its uncertainties. Traditionally, there have been two main routes for determining H_0. First, H_0 can be measured locally through the distance-ladder method. Distances to galaxies in the Hubble flow, where peculiar velocities are insignificant (the motion of galaxies is almost entirely due to the expansion of the Universe), can be measured using Type Ia supernovae (SNe Ia; e.g. Minkowski 1941; Elias et al. 1985; Filippenko 1997; Howell 2011, and references therein). For sufficiently nearby SN Ia host galaxies where individual stars can be resolved with the *Hubble Space Telescope (HST)*, the distances can be determined (and hence the peak luminosities of the SNe Ia can be calibrated) through measurements of Cepheid variable stars (Freedman et al. 2001; Sandage et al. 2006; Riess et al. 2009; Freedman & Madore 2010; Riess et al. 2011, 2016, 2018a,b; Burns et al. 2018; Dhawan, Jha & Leibundgut 2018; Riess et al. 2019) or the tip of the red giant branch (TRGB) in the Hertzsprung–Russell diagram (Madore, Mager & Freedman 2009; Jang & Lee 2017a,b; Freedman et al. 2019; Yuan et al. 2019). Cepheids and TRGBs can, in turn, be calibrated to geometric anchor distances like Milky Way Cepheid parallaxes (Benedict et al. 2007; Riess et al. 2014; Casertano et al. 2016),

★ E-mail: tdejaeger@berkeley.edu
† Bengier Postdoctoral Fellow.
‡ Marc J. Staley Graduate Fellow.
§ Miller Senior Fellow.

Keplerian motion of masers in NGC 4258 (Humphreys et al. 2013; Reid, Pesce & Riess 2019), or detached eclipsing binary stars in the Large Magellanic Cloud (Pietrzyński et al. 2013). Using this distance-ladder technique, the uncertainty in the measurement of H_0 has improved from ∼10 per cent (Freedman et al. 2001) to <2 per cent (Riess et al. 2019) during the last 20 yr. Currently, the most precise estimate of the H_0 is 74.03 ± 1.42 km s^{-1} Mpc^{-1} (Riess et al. 2019).

Secondly, H_0 can be predicted using the sound horizon observed from the cosmic microwave background radiation (CMB; e.g. Fixsen et al. 1996; Jaffe et al. 2001; Bennett et al. 2003; Spergel et al. 2007; Planck Collaboration VI 2018). However, H_0 cannot be constrained directly from CMB observations. While the local H_0 value at redshift $z \approx 0$ is obtained using the distance ladder from Hubble-flow SNe Ia ($z \approx 0.02$–0.15) using calibrated objects for each step, the second value is obtained using data at $z \approx 1100$ and extrapolated to $z \approx 0$ based on the physics of the early Universe. Assuming a flat λcold dark matter (ΛCDM) cosmological model, Planck Collaboration VI (2018) obtained a value of $H_0 = 67.4 \pm 0.5$ km s^{-1} Mpc^{-1}. A consistent value is also found when an intermediate-redshift rung and the inverse distance ladder method are used. For example, using baryon acoustic oscillations (BAO) calibrated from the CMB to anchor SNe Ia at $z > 0.1$, Macaulay et al. (2019) obtained $H_0 = 67.8 \pm 1.3$ km s^{-1} Mpc^{-1}.

Although the two H_0 values from opposite ends of the Universe agree to within 10 per cent, their error bars do not overlap and a discrepancy of $\sim 4.4\sigma$ is seen with SNe Ia (Riess et al. 2019) (and even greater significance, exceeding 6σ, when other nearby-universe techniques are combined; Riess 2020). This disagreement does not appear to be due to known systematic errors. Independent reanalyses of the Riess et al. (2016) data have shown minimal differences (Cardona, Kunz & Pettorino 2017; Zhang et al. 2017; Burns et al. 2018; Dhawan et al. 2018; Feeney, Mortlock & Dalmasso 2018; Follin & Knox 2018), and as more data and independent methods are used, the discrepancy is increasing (Riess et al. 2019). This significant tension between both measurements could arise from relativistic particles (dark radiation), non-zero curvature, early dark energy, increasing dark energy, or new fundamental physics.

However, to confirm the 'H_0 tension', it is important to develop as many independent methods as possible, having different systematic errors (see Riess 2020 for a recent review). For example, a novel measurement of H_0 has been made using quasars that are strongly gravitationally lensed into multiple images and the time-delay distance technique (Bonvin et al. 2017; Wong et al. 2019). From their analysis of multiply imaged quasars, the H0LiCOW collaboration (Bonvin et al. 2017) has measured a value of $73.3^{+1.7}_{-1.8}$ km s^{-1} Mpc^{-1} (Wong et al. 2019), consistent with the most recent local distance-ladder measurements (Riess et al. 2019). Additionally, the Megamaser Cosmology Project, using geometric distance measurements to megamaser-hosting galaxies, obtained an independent H_0 value of 73.9 ± 3.0 km s^{-1} Mpc^{-1} (Pesce et al. 2020). Other techniques such as 'standard sirens' from merger events detected through gravitational waves (Abbott et al. 2017) are also promising, but their current precision is not sufficient to put strong constraints; there is only a single electromagnetic gravitational-wave counterpart detection ($H_0 = 70^{+12}_{-8}$ km s^{-1} Mpc^{-1}). However, even 'dark sirens' that have no known electromagnetic detection have potential (Vasylyev & Filippenko 2020).

Needing approaches independent of SNe Ia, we study the use of SNe II as cosmological standardisable candles (de Jaeger et al. 2020). Observationally, SNe II are characterized by the presence of strong hydrogen features in their spectra (see Filippenko 1997, 2000 and Gal-Yam 2017 for overviews), and a plateau of varying steepness in their light curves (Barbon, Ciatti & Rosino 1979; Anderson et al. 2014; Galbany et al. 2016) during the hydrogen recombination phase. Their use as cosmic distance indicators is mainly motivated by the fact that they are more abundant than SNe Ia (Li et al. 2011; Graur et al. 2017) and their progenitors and environments are better understood than those of SNe Ia. It is now accepted that SN II progenitors arise from only one stellar population (red supergiant stars) for which the explosion mechanism is reasonably well understood (Woosley & Weaver 1995; Janka 2001; Janka et al. 2007).

At first sight, the SN II family displays a large range of peak luminosities (more than 2 mag); however, as for SNe Ia, their luminosities can be calibrated. To date, different theoretical and empirical SN II distance-measurement methods have been proposed and tested (e.g. Nugent & Hamuy 2017, and references therein). First, the expanding photosphere method (EPM) based on the relation between the angular size and the ratio between its observed and theoretical flux was developed by Kirshner & Kwan (1974). Following this method, several empirical methods have developed: the standard candle method based on the correlation between the luminosity and the expansion velocities (SCM; Hamuy & Pinto 2002; de Jaeger et al. 2020), the photospheric magnitude method, which corresponds to a generalization of the SCM (PMM; Rodríguez, Clocchiatti & Hamuy 2014; Rodríguez et al. 2019), and the photometric colour method, which uses the relation between the luminosity and the slope of the plateau (PCM; de Jaeger et al. 2015, 2017b). Using those techniques, H_0 values of 73 ± 13 km s^{-1} Mpc^{-1} (EPM; Schmidt et al. 1994), 69 ± 16 km s^{-1} Mpc^{-1} (SCM; Olivares E et al. 2010), and $\sim 71 \pm 8$ km s^{-1} Mpc^{-1} (PMM in the *V* band; Rodríguez et al. 2019) have been derived, but their precisions are not yet comparable to those of *Planck* or SNe Ia owing to a lack of SNe II in the Hubble flow, as well as to a small number of Cepheids or resolved red giants in SN II host galaxies.

In this work, we increase the number of calibrators and use the largest SN II sample in the Hubble flow to derive H_0 with a precision of ∼6.5 per cent (statistical). Section 2 contains a description of the SN data, and in Section 3, we present the methods used to derive H_0. We discuss our results in Section 4 and summarize our conclusions in Section 5.

2 DATA SAMPLE

For our analysis, we use SNe II from different surveys: the Carnegie Supernova Project-I (CSP-I[1]; Hamuy et al. 2006), the Lick Observatory Supernova Search (LOSS) with the 0.76 m Katzman Automatic Imaging Telescope (KAIT[2]; Filippenko et al. 2001), the Sloan Digital Sky Survey-II SN Survey (SDSS-II[3]; Frieman et al. 2008), the Supernova Legacy Survey (SNLS[4]; Astier et al. 2006; Perrett et al. 2010), the Dark Energy Survey Supernova Programme (DES-SN[5]; Bernstein et al. 2012), and the Subaru Hyper-Suprime Cam Survey (SSP-HSC; Miyazaki et al. 2012; Aihara et al. 2018). We also add SN 2009ib (Takáts et al. 2015), a nearby SN II for which we have an SN host distance measurement from Cepheids estimated

[1] http://csp.obs.carnegiescience.edu/
[2] http://w.astro.berkeley.edu/bait/kait.html
[3] http://classic.sdss.org/supernova/aboutsupernova.html
[4] http://cfht.hawaii.edu/SNLS/
[5] https://portal.nersc.gov/des-sn/

by the SH0ES[6] team (A. G. Riess, 2020, private communication). All of the data have already been used in different cosmological studies (Poznanski et al. 2009; Poznanski, Nugent & Filippenko 2010; D'Andrea et al. 2010; de Jaeger et al. 2015, 2017a,b, 2020) and a complete description of the surveys is given by Poznanski et al. (2009) (KAIT-P09), D'Andrea et al. (2010) (SDSS-SN), de Jaeger et al. (2015) (CSP-I), de Jaeger et al. (2017a) (SNLS, HSC), Ganeshalingam et al. (2010), Stahl et al. (2019), de Jaeger et al. (2019) (KAIT-d19), and de Jaeger et al. (2020) (DES-SN).

Following de Jaeger et al. (2020), our method is applied at 43 d after the explosion, and only SNe II with an explosion date uncertainty smaller than 10 d are selected. Additionally, since in this work we use the SCM, at least one spectrum per SN is needed to measure the photospheric expansion velocity. After these cuts, our sample consists of 125 SNe II: 49 (CSP-I) + 13 (SDSS-SN) + 4 (SNLS) + 12 (KAIT-P09) + 30 (KAIT-d19) + 15 (DES-SN) + 1 (HSC) + 1 (SN 2009ib). Among these 125 SNe II, 89 SNe II have $z > 0.01$.

Note that all of the CMB redshifts ($z_{\rm CMB}$) were obtained from the NASA/IPAC Extragalactic Database (NED[7]) and were corrected to account for peculiar flows ($z_{\rm corr}$) induced by visible structures using the model of Carrick et al. (2015). A residual peculiar velocity uncertainty of 250 km s^{-1} is also assumed.

3 METHODS

3.1 SN II standardization

To calibrate SNe II, the SCM is applied; see de Jaeger et al. (2020) for a full description of the method. Briefly, we use the observed correlations between SN II luminosity and photospheric expansion velocity during the plateau phase as well as the colour to correct the SN II magnitude. Thus, for each SN, the corrected magnitude can be written as

$$m^X_{\rm corr} = m_X + \alpha \log_{10}\left(\frac{v_{\rm H\beta}}{\langle v_{\rm H\beta}\rangle}\right) - \beta(c - \langle c\rangle), \quad (1)$$

where X is the X-band filter, m is the apparent magnitude at 43 d, c is the colour ($\langle c\rangle$ is the average colour), and $v_{H\beta}$ is the velocity measured using Hβ absorption ($\langle v_{\rm H\beta}\rangle$ is the average value). To determine the best-fitting parameters (α and β) and to derive the Hubble diagram, a Monte Carlo Markov Chain (MCMC) simulation is performed using the PYTHON package EMCEE developed by Foreman-Mackey et al. (2013). For more details, the reader is referred to equations (1), (2), and (3) of de Jaeger et al. (2020).

Note that all magnitudes were simultaneously corrected for Milky Way extinction ($A_{V,\rm G}$; Schlafly & Finkbeiner 2011), redshifts due to the expansion of the Universe (K-correction; Oke & Sandage 1968; Hamuy et al. 1993; Kim, Goobar & Perlmutter 1996; Nugent, Kim & Perlmutter 2002), and differences between the photometric systems (S-correction; Stritzinger et al. 2002) using the cross-filter K-corrections defined by Kim et al. (1996). More details regarding these correction are given by Nugent et al. (2002), Hsiao et al. (2007), de Jaeger et al. (2017b), and references therein.

[6]'Supernovae, H_0 for the Equation of State of Dark Energy'; Riess et al. (2011)

[7]http://ned.ipac.caltech.edu/

3.2 Calibrators

In our low-redshift samples (CSP-I, KAIT, and SN 2009ib), six SNe II have direct or indirect host-galaxy distance measurements from Cepheids, as follows:

(i) SN 1999em in NGC 1637 for which the distance modulus derived by Leonard et al. (2003) has been updated using the new Large Magellanic Cloud (LMC) distance (Pietrzyński et al. 2019) and an LMC to Milky Way Cepheid abundance difference of 0.30 dex (Riess et al. 2019). The distance modulus used in this work is $\mu = 30.26 \pm 0.09$ mag. Note that the metallicity term for optical Cepheid measurements used by Leonard et al. (2003) was 0.24 mag dex^{-1}.

(ii) SN 1999gi in NGC 3184 ($\mu = 30.64 \pm 0.11$ mag; updated from Leonard et al. 2002 using the new LMC distance), which is estimated through the average of the Cepheid distances of two galaxies (NGC 3319, $\mu = 30.60 \pm 0.08$ mag; NGC 3198, $\mu = 30.68 \pm 0.08$ mag; updated from Freedman et al. 2001) associated with the same galaxy group (Tully & Fisher 1988).

(iii) SN 2005ay in NGC 3998 ($\mu = 31.74 \pm 0.07$ mag; Riess et al. 2016), which is measured indirectly from the Cepheid distance of NGC 3982, also a member of the Ursa Major Group.

(iv) SN 2008bk ($\mu = 27.66 \pm 0.11$ mag; Zgirski et al. 2017) in NGC 7793.

(v) SN 2009ib in NGC 1559 ($\mu = 31.416 \pm 0.049$ mag; A. G. Riess, 2020, private communication). This value is consistent with the one derived by Huang et al. (2020) using Mira variable stars ($\mu = 31.41 \pm 0.05$ (stat) ± 0.052 (sys) mag.

(vi) SN 2012aw in NGC 3351 ($\mu = 29.82 \pm 0.09$ mag;) updated from Kanbur et al. (2003) following the prescriptions used for SN 1999em in NGC 1637.

In addition to these six SNe II with Cepheid measurements, we also have three SNe II with TRGB distance derivations:

(i) SN 2004et in NGC 6946 ($\mu = 29.38 \pm 0.09$ mag; Anand, Rizzi & Tully 2018).

(ii) SN 2005cs in NGC 5194 (M51; $\mu = 29.62 \pm 0.09$ mag; updated from McQuinn et al. 2017).

(iii) SN 2013ej in NGC 628 (M74; $\mu = 29.90 \pm 0.10$ mag; updated from McQuinn et al. 2017).

For SN 2005cs and SN 2013ej, to convert the TRGB luminosities to distance moduli, we used a zero-point calibration of -4.01 from outer and halo fields in NGC 4258 (Reid et al. 2019) instead of -4.06 for typical TRGB colour (Rizzi et al. 2007).

A summary of all the calibrators available in this work can be found in Table 1. To homogenize our calibrators, we remove two objects from this analysis. First, SN 2008bk, a low-luminosity SN II (Van Dyk et al. 2012), the only object for which the distance was obtained using ground-based (and not *HST*) observations (and then only of 11 Cepheids), and we cannot determine if these zero-points are consistent with those from *HST*. Secondly, SN 2004et has the largest Milky Way extinction ($A_{V,\rm G} \approx 1.0$ mag), making it very unreliable. Note that Rodríguez et al. (2019) also identified SN 2004et as an outlier and they removed it from their calibrator sample.

3.3 H_0 derivation from SNe II

The method for determining H_0 can be divided into three steps. First, we need to calibrate the SN II apparent magnitudes by deriving α and β from equation (1). To minimize the effect of peculiar-galaxy

Table 1. Calibrator sample.

SN name	Host galaxy	μ (mag)	Calibrator	Used	References
SN 1999em	NGC 1637	30.26 ± 0.09	Cepheids	Yes	Updated from Leonard et al. (2003)
SN 1999gi	NGC 3184	30.64 ± 0.11	Cepheids	Yes	Updated from Leonard et al. (2002)
SN 2004et	NGC 6946	29.38 ± 0.09	TRGB	No	Anand et al. (2018)
SN 2005ay	NGC 3998	31.74 ± 0.07	Cepheids	Yes	Riess et al. (2016)
SN 2005cs	NGC 5194/M51	29.62 ± 0.09	TRGB	Yes	Updated from McQuinn et al. (2017)
SN 2008bk	NGC 7793	27.66 ± 0.11	Cepheids	No	Zgirski et al. (2017)
SN 2009ib	NGC 1559	31.42 ± 0.05	Cepheids	Yes	A. G. Riess (2020), private communication
SN 2012aw	NGC 3351	29.82 ± 0.09	Cepheids	Yes	Updated from Kanbur et al. (2003)
SN 2013ej	NGC 628/M74	29.90 ± 0.10	TRGB	Yes	Updated from McQuinn et al. (2017)

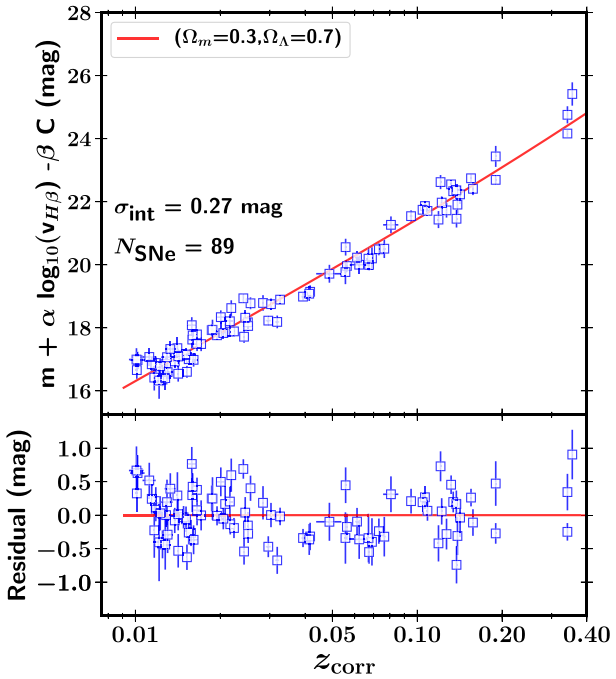

Figure 1. Hubble diagram (top) and residuals from the ΛCDM model (bottom) using the SCM as applied to our sample of 89 SNe II in the Hubble flow. $z_{\rm corr}$ corresponds to the CMB redshifts corrected to account for peculiar flows. The red solid line is the Hubble diagram for the ΛCDM model ($\Omega_{\rm m} = 0.3$, $\Omega_\Lambda = 0.7$) and $H_0 = 75.8\,{\rm km\,s^{-1}\,Mpc^{-1}}$ (see Section 4.1). This Hubble diagram was built using the i-band magnitude, $(r-i)$ colour, and at 43 d after the explosion. We present the number of SNe II available at this epoch ($N_{\rm SNe}$) and the intrinsic dispersion ($\sigma_{\rm int}$). Note that the error bars do not include the intrinsic dispersion.

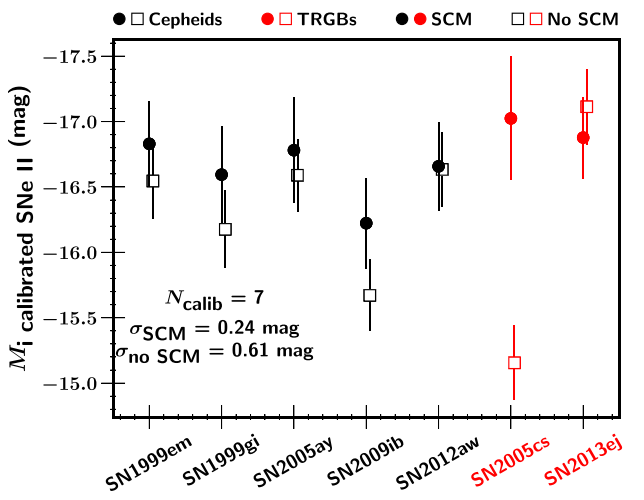

Figure 2. Absolute i-band magnitude 43 d after the explosion for the calibrators based on Cepheid distances (black) or the TRGB (red). The empty squares are the absolute magnitudes without applying the SCM, while the filled circles are with velocity and colour corrections. We also present the standard deviation with and without SCM.

motions, we select SNe II located in the Hubble flow, with $z_{\rm corr} > 0.01$ (89 objects). Fig. 1 shows the Hubble diagram for this sample. The uncertainties associated with the corrected magnitudes are

$$\sigma^2_{m_{\rm corr}} = \sigma^2_m + \left(\frac{\alpha\sigma_{v_{\rm H\beta}}}{\ln 10 v_{\rm H\beta}}\right)^2 + (\beta\sigma_{(r-i)})^2 + \sigma^2_z, \quad (2)$$

where σ^2_z includes the redshift measurement uncertainties and a peculiar velocity error of $250\,{\rm km\,s^{-1}}$. To the total uncertainty, a free parameter $\sigma_{\rm int}$ is added to take into account the unmodelled intrinsic SN II scatter. A value of 0.27 mag is derived, consistent with previous SCM research (Poznanski et al. 2009; D'Andrea et al. 2010; de Jaeger et al. 2017a, 2020). The values of α and β used to correct the SN II apparent magnitudes are respectively $3.95^{+0.43}_{-0.42}$ and 1.07 ± 0.28 (see Section 4.1). If we assume that the colour–magnitude relation is due to extrinsic factors, the total-to-selective extinction ratio (R_V) can be obtained from β. We find a lower $R_V \approx 1$ than for SNe Ia (Folatelli et al. 2010), but the low value could be due to intrinsic magnitude-colour not properly modelled. Recently, de Jaeger et al. (2018) suggested that the majority of SN II observed colour diversity is intrinsic and not produced by host-galaxy dust extinction. Note that these parameters depend on the sample chosen; in Section 4.2, we investigate their effects on the derived value of H_0.

For the last two steps, we follow the work done by Dhawan et al. (2018) and adapt their PYTHON programmes[8] to our SN II sample. We derive the absolute magnitudes of all calibrators, $M_i^{\rm cal}$ ($\sigma_{M_i^{\rm cal}}$), using the Cepheid and TRGB distances from Table 1 and by correcting their apparent magnitudes with the α and β derived previously:

$$M_i^{\rm cal} = m_i^{\rm cal} + \alpha \log_{10}\left(v_{\rm H\beta}\right) - \beta(r-i) - \mu_{\rm cal}, \quad (3)$$

$$\sigma_{M_i^{\rm cal}} = \sigma^2_{m_i} + \left(\frac{\alpha}{\ln 10}\frac{\sigma_{v_{\rm H\beta}}}{v_{\rm H\beta}}\right)^2 + (\beta\sigma_{(r-i)})^2 + \sigma^2_{\mu_{\rm cal}} + \sigma^2_{\rm int}. \quad (4)$$

The absolute magnitudes for all seven calibrators are displayed in Fig. 2. Note that the uncertainties include the intrinsic scatter $\sigma_{\rm int}$. The calibrators have an average weighted absolute magnitude

[8] https://github.com/sdhawan21/irh0/blob/master/full-analysis.ipynb

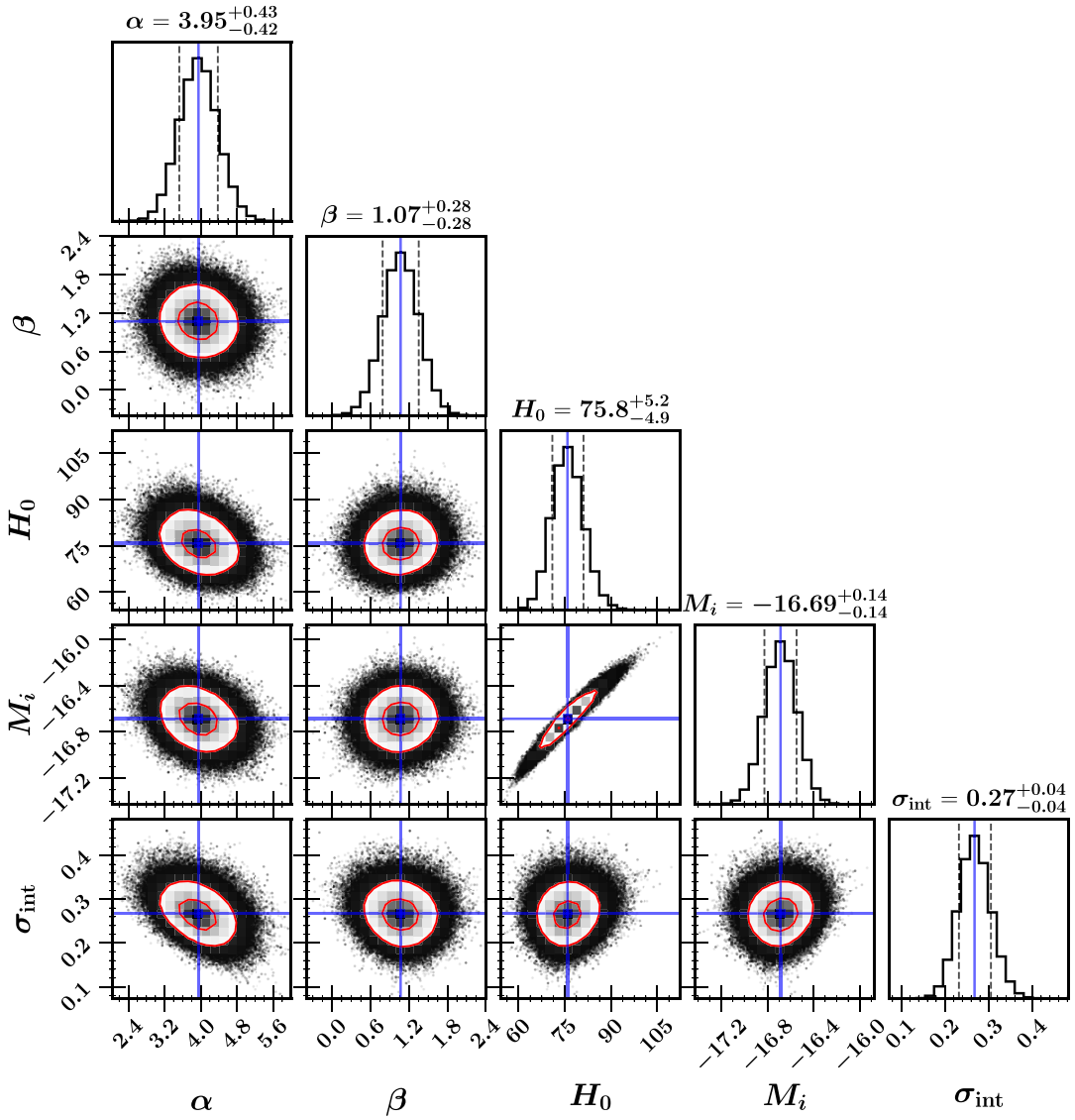

Figure 3. Corner plot showing all of the one- and two-dimensional projections. Data points are shown as grey-scale points and red contours are given at 1σ and 2σ (which corresponds in two dimensions to the 39 and 86 per cent of the volume). The five free parameters of our model are plotted: α, β, H_0, M_i, and $\sigma_{\rm int}$. For each parameter, the median value and the 16th and 84th percentile difference are shown. To make this figure, we used the corner-plot package (triangle.py v0.1.1. Zenodo. 10.5281/zenodo.11020).

of -16.69 mag with a dispersion of $\sigma_{\rm cal} = 0.24$ mag. The dispersion is slightly larger than that obtained using SNe Ia (0.16 mag; Riess et al. 2016; Dhawan et al. 2018) but biased by the low-statistics number of calibrators (19 calibrators used for SNe Ia). When the SCM is not applied, the dispersion increases to 0.61 mag, demonstrating the utility of the SCM. SN 2005cs exhibits the largest difference with or without SCM because SN 2005cs is a low-luminosity SN II (Pastorello et al. 2006) and has small ejecta velocities, and therefore the largest $\alpha \log_{10}$ (vel/$\langle$vel$\rangle$) corrections.

It is important to note that on average, the absolute magnitude for the TRGBs is brighter ($N = 2$, -16.93 ± 0.28 mag) than for the Cepheids ($N = 5$, -16.62 ± 0.16 mag). As Jang & Lee (2017a) showed that TRGB distances are in good agreement with the Cepheid distances derived by Riess et al. (2011), Riess et al. (2016), the difference in absolute magnitude could be explained by a small-number statistics.

The third and last step consists of combining the calibrator and the Hubble-flow samples. The calibrator sample will constrain the absolute magnitude M_i, while the Hubble-flow sample is used to determined the intercept of the SN II magnitude–redshift relation (zero point). In practice,

$$\mu = m_i - M_i = 5 \log_{10}(d_{\rm L}) + 25, \tag{5}$$

where the luminosity distance ($d_{\rm L}$) in Mpc is defined by its kinematic expression as

$$d_{\rm L} \approx \frac{cz}{{\rm H}_0} \left(1 + \frac{(1 - q_0)z}{2} + \frac{\left(1 - q_0 - 3q_0^2 + j_0\right) z^2}{6} \right). \tag{6}$$

As defined by Riess et al. (2007), q_0 is the present acceleration ($q_0 = -0.55$) and j_0 is the prior deceleration ($j_0 = 1$). Using equations (5)

Table 2. Free-parameter values for different sample choices.

Sample	Cali	$N_{\rm cali}$	$\sigma_{\rm cali}$ (mag)	$N_{\rm SNe}$	α	β	H_0 (km s^{-1} Mpc^{-1})	M_i (mag)	$-5\,a_i$ (mag)	$\sigma_{\rm int}$ (mag)	ΔH_0
Original	C+T	7	0.24	89	$3.95^{+0.43}_{-0.42}$	1.07 ± 0.28	$75.8^{+5.2}_{-4.9}$	-16.69 ± 0.14	-1.08 ± 0.04	0.27 ± 0.04	···
$v_{\rm pec} = 150$ km s^{-1}	C+T	7	0.24	89	$3.94^{+0.43}_{-0.42}$	$1.07^{+0.28}_{-0.27}$	$75.6^{+5.3}_{-4.9}$	-16.69 ± 0.14	-1.08 ± 0.04	0.28 ± 0.04	0.3%
$z_{\rm corr} > 0.023$	C+T	7	0.29	47	$4.07^{+0.65}_{-0.63}$	$0.41^{+0.48}_{-0.46}$	$77.8^{+6.2}_{-5.7}$	-16.79 ± 0.16	-1.24 ± 0.05	$0.28^{+0.05}_{-0.04}$	2.6%
$0.023 > z_{\rm corr} > 0.15$	C+T	7	0.27	40	$4.08^{+0.74}_{-0.72}$	$0.71^{+0.50}_{-0.49}$	$78.2^{+6.3}_{-5.8}$	-16.74 ± 0.16	-1.20 ± 0.06	0.29 ± 0.05	3.2%
$z_{\rm corr} > 0.01$	C	5	0.21	89	$4.02^{+0.46}_{-0.45}$	$1.05^{+0.28}_{-0.29}$	$78.5^{+6.3}_{-5.8}$	-16.61 ± 0.16	-1.08 ± 0.04	0.27 ± 0.04	3.6%
$z_{\rm corr} > 0.01$	T	2	0.08	89	$3.96^{+0.44}_{-0.42}$	$1.00^{+0.30}_{-0.29}$	$69.0^{+9.1}_{-8.2}$	-16.89 ± 0.27	-1.09 ± 0.04	0.27 ± 0.04	9.0%
−09ib	C	4	0.10	89	$4.00^{+0.45}_{-0.44}$	$1.01^{+0.28}_{-0.29}$	$74.9^{+6.7}_{-6.1}$	-16.71 ± 0.18	-1.08 ± 0.04	0.27 ± 0.04	1.2%
−09ib	C+T	6	0.14	89	$3.94^{+0.42}_{-0.41}$	$1.03^{+0.28}_{-0.29}$	$72.9^{+5.4}_{-5.0}$	-16.77 ± 0.15	-1.08 ± 0.04	0.27 ± 0.04	3.8%
+04et, 08bk	C+T	9	0.35	89	$4.16^{+0.43}_{-0.42}$	$1.15^{+0.28}_{-0.29}$	$74.4^{+4.8}_{-4.5}$	-16.73 ± 0.13	-1.08 ± 0.04	0.27 ± 0.03	1.8%
bootstrap	C+T	7	0.18	89	$3.96^{+0.45}_{-0.44}$	$1.04^{+0.28}_{-0.27}$	$75.4^{+6.8}_{-6.5}$	-16.70 ± 0.18	-1.08 ± 0.04	0.27 ± 0.04	0.5%
CSP-I	C+T	7	0.23	37	$3.86^{+0.58}_{-0.56}$	$1.18^{+0.41}_{-0.40}$	$76.2^{+5.4}_{-4.9}$	-16.62 ± 0.14	-1.03 ± 0.05	0.24 ± 0.04	0.5%
KAIT	C+T	7	0.27	19	$4.75^{+0.88}_{-0.93}$	$1.95^{+0.53}_{-0.56}$	$74.7^{+6.1}_{-5.6}$	-16.59 ± 0.14	-0.96 ± 0.08	0.26 ± 0.07	1.5%
CSP-I+KAIT	C+T	7	0.23	56	$4.10^{+0.54}_{-0.50}$	$1.39^{+0.34}_{-0.35}$	$75.6^{+5.4}_{-5.0}$	-16.62 ± 0.14	-1.01 ± 0.05	0.26 ± 0.05	0.3%
'high-z'	C+T	7	0.26	33	$3.61^{+0.67}_{-0.64}$	$0.56^{+0.50}_{-0.49}$	$78.1^{+6.0}_{-5.6}$	-16.74 ± 0.15	-1.21 ± 0.06	0.27 ± 0.05	3.0%

Effect of systematic errors on the best-fitting values using the SCM and different samples. Original line corresponds to the values obtained in Section 4.1. We try different cuts in redshift ($z_{\rm corr}$), surveys (e.g. only CSP-I, only KAIT, CSP-I+KAIT, high-z SDSS+SNLS+DES+HSC), calibrators [Cepheids (C) and/or TRGBs (T)], and also remove or add some calibrators (e.g. −09ib for SN 2009ib; +04et, 08bk for SN 2004et, SN 2008bk). Bootstrap line corresponds to the average value obtained when performed a bootstrap resampling of the set of calibrators, with replacement using seven calibrators. For each parameter, the median value with the 16th and 84th percentile differences are given (uncertainties are only statistical). For the bootstrap line, the median and the standard deviation added in quadrature to the mean of the uncertainties obtained for each parameter are written. The last column, ΔH_0, corresponds to the percentage difference from the original.

and (6), we can extract H_0 as

$$\log_{10} H_0 = \frac{M_i + 5\,a_i + 25}{5}, \quad (7)$$

where a_i is the intercept measured from the Hubble-flow sample and M_i is the absolute SN II i-band magnitude (at 43 d) derived using our calibrator sample. Following Dhawan et al. (2018), to derive H_0, we use the PYTHON package EMCEE developed by Foreman-Mackey et al. (2013) and fit a joint model which combined the Hubble-flow and calibrator samples. The likelihood will evaluate how close the calibrators are to the mean absolute magnitude, and simultaneously how close the Hubble-flow SN II absolute magnitudes are to the mean absolute magnitude given a value of H_0. In this model, α, β, H_0, M_i, and $\sigma_{\rm int}$ are free parameters, and a_i can be obtained using equation (7). We run the MCMC simulation with 300 walkers and 2000 steps, and the priors are uniform for α, $\beta \neq 0$, $H_0 > 0$, and $M_i < 0$, and scale free for $0.0 < \sigma_{\rm int}$ with $p(\sigma_{\rm int}) = 1/\sigma_{\rm int}$.

4 RESULTS

4.1 Hubble constant

In Fig. 3, the one- and two-dimensional projections of the five free parameters of our model (α, β, H_0, M_i, and $\sigma_{\rm int}$) are shown. For the Hubble-flow SN II sample, we use all SNe II with $z_{\rm corr} > 0.01$ ($N = 89$) and the seven calibrators described in Table 1. We obtain a median value of $H_0 = 75.8^{+5.2}_{-4.9}$ km s^{-1} Mpc^{-1}, where the uncertainties are only statistical. With a ∼6.7 per cent statistical uncertainty, this value is the most precise ever obtained using SNe II.

Our result is consistent with the local H_0 determined from SNe Ia (74.03 ± 1.42 km s^{-1} Mpc^{-1}; Riess et al. 2019) and shows a discrepancy of $\sim 1.7\sigma$ with the high-redshift value ($H_0 = 67.4 \pm 0.5$ km s^{-1} Mpc^{-1}; Planck Collaboration VI 2018). The median absolute i-band magnitude 43 d after the explosion of the calibrators is $M_i = -16.69 \pm 0.14$ mag, while the intercept $-5\,a_i$ has a value of -1.08 ± 0.04 mag (derived using equation 7). Finally, an intrinsic scatter $\sigma_{\rm int} = 0.27 \pm 0.04$ mag is obtained, consistent with previous SCM work where the community derived a value between 0.25 and 0.33 (Poznanski et al. 2009; D'Andrea et al. 2010; Olivares E et al. 2010; de Jaeger et al. 2017a, 2020).

4.2 Systematic uncertainties

In this section, we investigate the effect of our different cuts and calibrators on H_0; the results are summarized in Table 2 and Fig. 4.

First, if we change the peculiar velocity error to 150 km s^{-1} (versus 250 km s^{-1}), H_0 slightly changes to $75.6^{+5.3}_{-4.9}$ km s^{-1} Mpc^{-1}, only a difference of 0.3 per cent (0.2 km s^{-1} Mpc^{-1}). Then, if we select only the SNe II with $z_{\rm corr} > 0.023$ (Riess et al. 2011), the number of SNe II available for the Hubble diagram decreases to 47 and H_0 increases to $77.8^{+6.2}_{-5.7}$ km s^{-1} Mpc^{-1}, a difference of 2.6 per cent (1.9 km s^{-1} Mpc^{-1}). The difference can be explained by peculiar velocities that are not perfectly corrected. Increasing the sample size of SNe II with $z_{\rm corr} > 0.023$ will reduce the systematic uncertainties caused by peculiar motions.

The largest difference in H_0 is seen when different calibrators are used. If only the Cepheids are selected as calibrators, H_0 increases to $78.5^{+6.3}_{-5.8}$ km s^{-1} Mpc^{-1}, a difference of 3.2 per cent compared with the original sample. With the Cepheids, a slight difference of 0.5 per cent from the original sample is also seen for the absolute i-band magnitude: -16.61 ± 0.16 mag. As discussed in Section 3.3 and Fig. 2, SN II magnitudes calibrated with TRGBs are, on an average, brighter than those calibrated using Cepheids. Therefore, if only the TRGBs are used as calibrators, the absolute i-band magnitude increases to -16.89 ± 0.27 mag, a difference of 0.20 mag from the original sample. Although the dispersion decreases to 0.08 mag (instead of 0.24 mag), H_0 decreases to $69.0^{+9.1}_{-8.2}$ km s^{-1} Mpc^{-1}, a difference of 9.0 per cent. However, the large difference is driven by small-number statistics.

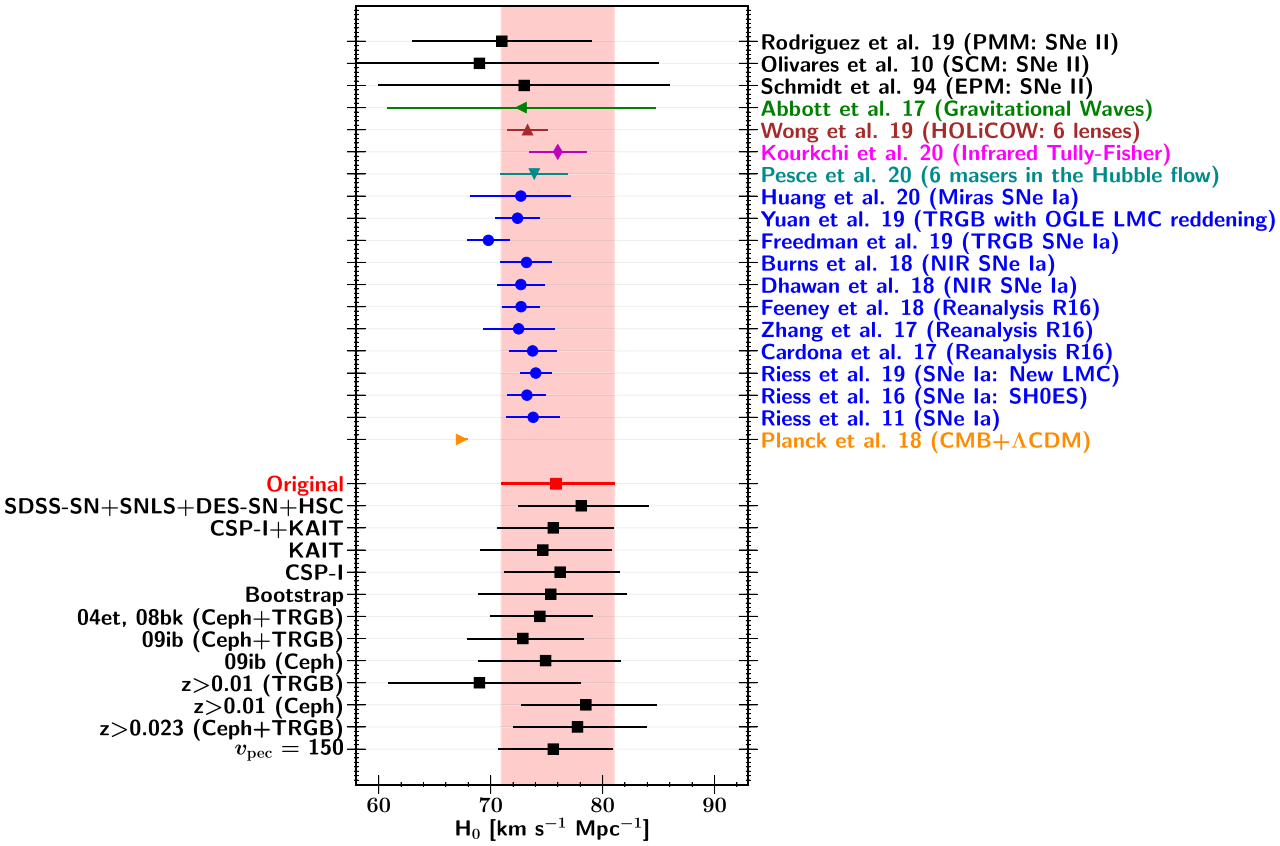

Figure 4. Comparison of the H_0 value derived in this work using SNe II with different cuts or samples (bottom black squares). The red filled region corresponds to the value obtained from our 'original' sample ($z_{corr} > 0.01$, $v_{pec} = 250\,km\,s^{-1}$, and using our seven calibrators). We also added the local measurements from SNe Ia (blue circles) using optical colours (Riess et al. 2011, 2016, 2019), the Riess et al. 2016 data reanalysis (Cardona et al. 2017; Zhang et al. 2017; Feeney et al. 2018), using near-infrared (NIR) filters (Burns et al. 2018; Dhawan et al. 2018), with TRGB + SNe Ia (Freedman et al. 2019), TRGB + SNe Ia with OGLE LMC reddening (Yuan et al. 2019), and with Mira variables + SNe Ia (Huang et al. 2020). Published values using SNe II from Schmidt et al. (1994), Olivares E et al. (2010), and Rodríguez et al. (2019) are also shown (top black squares). H_0 values estimated using six masers in the Hubble flow (Pesce et al. 2020), infrared Tully–Fisher relation (Kourkchi et al. 2020), the independent methods of quasar strong lensing (Wong et al. 2019), and gravitational-wave sources (Abbott et al. 2017) are also presented (dark cyan down-pointing triangle, magenta diamond, brown up-pointing triangle, and green left-pointing triangle, respectively). Finally, the high-z value predicted by the CMB data + ΛCDM from Planck Collaboration VI (2018) is represented by an orange right-pointing triangle.

By removing the least luminous SN II (SN 2009ib; see Fig. 2) from the Cepheid sample, we derive a value smaller than that obtained with the original sample, $74.9^{+6.7}_{-6.1}$ km s^{-1} Mpc^{-1}, a difference of only 0.9 km s^{-1} Mpc^{-1} (∼1.2 per cent). However, the absolute-magnitude dispersion of the calibrators decreases to 0.10 mag (versus 0.21 mag) but with only 4 SNe II. We can also combine the Cepheid and TRGB samples after removing SN 2009ib. The calibrator absolute magnitude dispersion remains small (0.14 mag) and the H_0 derived presents a difference of only 2.9 km s^{-1} Mpc^{-1} (3.8 per cent). As a test, we also add the two calibrators (SN 2004et and SN 2008bk) removed from our calibrator set (see Section 3.2). With the nine calibrators, we obtain a value of $74.4^{+4.8}_{-4.5}$ km s^{-1} Mpc^{-1}, which differs by 1.4 km s^{-1} Mpc^{-1} (∼1.8 per cent).

To get a more realistic idea of the calibrator effects on H_0, we also perform a bootstrap resampling of the set of calibrators, with replacement (see Fig. 5). To explore all the possibilities (13!/7!6!), we run 1716 simulations and get an average value of 76.1 ± 4.2 km s^{-1} Mpc^{-1}. To compare with the original value, we take the median of these simulations, and as total uncertainty the standard deviation (4.2 km s^{-1} Mpc^{-1}) added in quadrature to the mean of the errors obtained for each simulation (+5.3 and −5.00 km s^{-1} Mpc^{-1}). We derive H_0 close to the original value: $75.4^{+6.8}_{-6.5}$ km s^{-1} Mpc^{-1}, differing by only 0.4 km s^{-1} Mpc^{-1} (∼0.5 per cent). The distribution displayed in Fig. 5 clearly shows that our H_0 value favours that obtained by Riess et al. (2019). The peak of our distribution matches H_0 from the local measurements using SNe Ia, while the distribution almost does not overlap the *Planck* + ΛCDM value. The fact that our distribution extends to large H_0 values (85–95 km s^{-1} Mpc^{-1}) is driven by SN 2009ib, which is the faintest calibrator. All the values larger than 85 km s^{-1} Mpc^{-1} were obtained when among the seven selected calibrators, SN 2009ib is used at least four times. For example, among the 1716 different possibilities, as we select seven SNe (with replacement) from our set of calibrators, for some combinations we used [SN 2009ib, SN 2009ib, SN 2009ib, SN 2009ib, X, Y, Z], where X, Y, and Z are SN 1999em, SN 1999gi, SN 2005ay, SN 2005cs, SN 2009ib, SN 2012aw, or SN 2013ej.

Finally, we can select different surveys to calibrate the SNe II. If we select only CSP-I (37 SNe II), H_0 is very consistent with the original sample value with a slight difference of 0.4 km s^{-1} Mpc^{-1} (∼0.5 per cent). Combining our two low-redshift

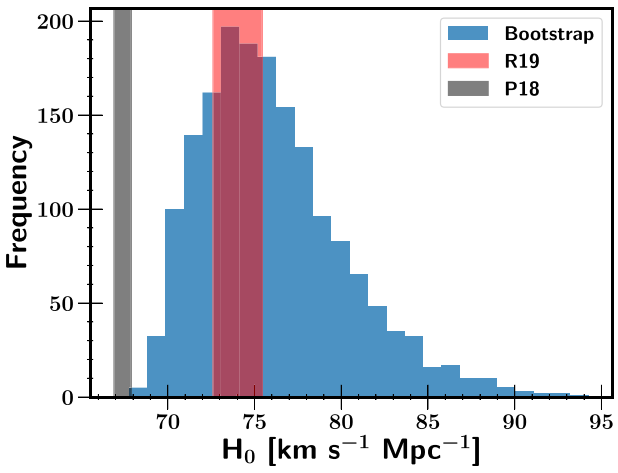

Figure 5. Histogram of our bootstrap resampling of the set of calibrators, with replacement. In total, 1716 simulations were performed and 25 bins are used. An average value of 76.1 ± 4.2 km s^{-1} Mpc^{-1} and a median value of 75.4 km s^{-1} Mpc^{-1} are derived. The red and black filled regions correspond to the H$_0$ values obtained by Riess et al. (2019) and Planck Collaboration VI (2018), respectively. None of the 1716 H$_0$ values are smaller than 67.4 km s^{-1} Mpc^{-1} (Planck Collaboration VI 2018) and only 3.5 per cent have a discrepancy smaller than 1σ (including only a systematic error of 2.8 km s^{-1} Mpc^{-1}).

samples (CSP-I and KAIT) or selecting only KAIT decreases the value to $74.7^{+6.1}_{-5.6}$ km s^{-1} Mpc^{-1} and $75.6^{+5.4}_{-5.0}$ km s^{-1} Mpc^{-1}, respectively; these are respective differences of 1.1 km s^{-1} Mpc^{-1} and 0.2 km s^{-1} Mpc^{-1} (1.5 and 0.3 per cent). If we select only the 'high-z' sample (SDSS-SN, SNLS, DES-SN, HSC), H$_0$ increases to $78.1^{+6.0}_{-5.6}$ km s^{-1} Mpc^{-1}, a difference of 2.3 km s^{-1} Mpc^{-1} (3.0 per cent).

From the standard deviation of 13 analysis variants presented in Table 2, we derive a systematic uncertainty of ∼2.5 km s^{-1} Mpc^{-1} (i.e. 3.3 per cent). To this systematic uncertainty, we also add, in quadrature, an uncertainty of ∼1.2 km s^{-1} Mpc^{-1} (1.5 per cent for the LMC in table 6 of Riess et al. 2019) owing to the error in the anchor measurements (anchor distance, mean of period–luminosity relation in anchor, zero-points anchor-to-hosts, and Cepheid metallicity). The total systematic uncertainty is ∼2.8 km s^{-1} Mpc^{-1} (i.e. 3.7 per cent). Thus, from our original sample, we obtain $H_0 = 75.8^{+5.2\,(\mathrm{stat})}_{-4.9\,(\mathrm{stat})} \pm 2.8\,(\mathrm{sys})$ km s^{-1} Mpc^{-1}. Our H$_0$ value (75.8 ± 5.8 km s^{-1} Mpc^{-1}) derived using SNe II is consistent (difference of 0.3σ) with the local measurements from SNe Ia (Riess et al. 2019), but shows a discrepancy of ∼1.4σ with the high-redshift results (Planck Collaboration VI 2018). Therefore, our value favours that obtained by Riess et al. (2019) (with a difference of only 1.8 km s^{-1} Mpc^{-1}) rather than that estimated by Planck Collaboration VI (2018) (with a difference of 8.4 km s^{-1} Mpc^{-1}). Note that the small calibrator set leads to large statistical uncertainty but leaves room for decreasing the total uncertainty. As a simple test, instead of selecting seven calibrators, we use each calibrator twice (14 calibrators in total). The final statistical uncertainty decreases from 5.1 (the average of 5.2 and 4.9) to 3.7 km s^{-1} Mpc^{-1} (25 per cent).

To summarize, in this work we only exchange SNe II for SN Ia to measure extragalactic distances; taking this study at face-value, there is no evidence that SNe Ia are the source of the H$_0$ tension. The probability $P(\mathrm{H}_0 \leq \mathrm{H}_{0,\,Planck})$ that our H$_0$ measurement from the bootstrap distribution (moved toward the *Planck* measurement by the systematic error) is at least as low as 67.4 km s^{-1} Mpc^{-1} (Planck Collaboration VI 2018) is only 4.5 per cent (see equation 10 of Pesce et al. 2020).

5 CONCLUSIONS

In this work, we show that SNe II have a role to play in the 'H$_0$ tension,' as they can be used to obtain extragalactic distances and provide an independent measurement of H$_0$. From SNe II and using only seven objects with Cepheid or TRGB independent host-galaxy distance measurements, we derive the most precise value of H$_0$ solely using SNe II: $\mathrm{H}_0 = 75.8^{+5.2}_{-4.9}$ km s^{-1} Mpc^{-1}, where the uncertainties are only statistical.

We also investigate the effect of our different cuts and calibrators on H$_0$ and estimate a systematic error of ∼2.8 km s^{-1} Mpc^{-1} (∼3.7 per cent). If we combine the systematic and the statistical errors, our value (75.8 ± 5.8 km s^{-1} Mpc^{-1}) is consistent with the local measurement (Riess et al. 2019), a difference of only 1.8 km s^{-1} Mpc^{-1}. On the other hand, our H$_0$ value differs by 1.4σ from the high-redshift results (Planck Collaboration VI 2018) – a difference of 8.4 km s^{-1} Mpc^{-1}. The probability that our H$_0$ measurement from the bootstrap distribution is at least as low as 67.4 km s^{-1} Mpc^{-1} (Planck Collaboration VI 2018) is only 4.5 per cent. Given that we only exchange SNe II for SNe Ia, this demonstrates that there is no evidence from our work that SNe Ia are the source of the H$_0$ tension. However, it will be interesting to apply the inverse distance-ladder method to SNe II (CMB+BAO) and compare with the value of H$_0$ obtained in this work (distance-ladder method). Recent studies calibrating BAO + SNe Ia from the Early Universe have obtained smaller Hubble constant values reinforcing the motion that the tension is an inconsistency between Late Universe geometry and Early Universe physics.

With the next generation of telescopes (e.g. the Vera C Rubin Observatory), we will be able to increase the number of calibrators and SNe II in the Hubble flow and thus improve the precision of H$_0$. For example, we showed that selecting only SNe II with $z > 0.023$ in our present sample generates an H$_0$ variation of ∼3 per cent.

ACKNOWLEDGEMENTS

We thank the referee for their comments on the manuscript, which helped improve it. Support for AVF's supernova research group at UC Berkeley has been provided by the NSF through grant AST-1211916, the TABASGO Foundation, Gary and Cynthia Bengier (TdJ is a Bengier Postdoctoral Fellow), Marc J. Staley (BES is a Marc J. Staley Graduate Fellow), the Christopher R. Redlich Fund, the Sylvia and Jim Katzman Foundation, and the Miller Institute for Basic Research in Science (UC Berkeley). LG was funded by the European Union's Horizon 2020 research and innovation programme under the Marie Skłodowska-Curie grant agreement no. 839090. This work has been partially supported by the Spanish grant PGC2018-095317-B-C21 within the European Funds for Regional Development (FEDER). The work of the CSP-I has been supported by the US NSF under grants AST-0306969, AST-0607438, and AST-1008343.

KAIT and its ongoing operation were made possible by donations from Sun Microsystems, Inc., the Hewlett-Packard Company, AutoScope Corporation, Lick Observatory, the US NSF, the University of California, the Sylvia & Jim Katzman Foundation, and the TABASGO Foundation. Research at Lick Observatory is partially supported by a generous gift from Google. This research used the

Savio computational cluster resource provided by the Berkeley Research Computing programme at UC Berkeley (supported by the UC Berkeley Chancellor, Vice Chancellor for Research, and Chief Information Officer).

This paper is based, in part, on data collected at the Subaru telescope and retrieved from the HSC data archive system, which is operated by the Subaru Telescope and Astronomy Data Center at the National Astronomical Observatory of Japan (NAOJ). The Hyper Suprime-Cam (HSC) collaboration includes the astronomical communities of Japan and Taiwan, and Princeton University. The HSC instrumentation and software were developed by the NAOJ, the Kavli Institute for the Physics and Mathematics of the Universe (Kavli IPMU), the University of Tokyo, the High Energy Accelerator Research Organization (KEK), the Academia Sinica Institute for Astronomy and Astrophysics in Taiwan (ASIAA), and Princeton University. Funding was contributed by the FIRST programme from the Japanese Cabinet Office, the Ministry of Education, Culture, Sports, Science and Technology (MEXT), the Japan Society for the Promotion of Science (JSPS), the Japan Science and Technology Agency (JST), the Toray Science Foundation, NAOJ, Kavli IPMU, KEK, ASIAA, and Princeton University.

The Pan-STARRS1 surveys (PS1) were made possible through contributions of the Institute for Astronomy, the University of Hawaii, the Pan-STARRS Project Office, the Max-Planck Society and its participating institutes, the Max Planck Institute for Astronomy, Heidelberg and the Max Planck Institute for Extraterrestrial Physics, Garching, The Johns Hopkins University, Durham University, the University of Edinburgh, Queen's University Belfast, the Harvard-Smithsonian Center for Astrophysics, the Las Cumbres Observatory Global Telescope Network Incorporated, the National Central University of Taiwan, the Space Telescope Science Institute, the National Aeronautics and Space Administration (NASA) under grant No. NNX08AR22G issued through the Planetary Science Division of the NASA Science Mission Directorate, the US NSF under grant AST-1238877, the University of Maryland, and Eotvos Lorand University (ELTE). This paper makes use of software developed for the Large Synoptic Survey Telescope. We thank the LSST Project for making their code available as free software at http://dm.lsst.org.

Some of the data presented herein were obtained at the W. M. Keck Observatory, which is operated as a scientific partnership among the California Institute of Technology, the University of California, and NASA; the observatory was made possible by the generous financial support of the WM Keck Foundation. This work is based in part on data produced at the Canadian Astronomy Data Centre as part of the CFHT Legacy Survey, a collaborative project of the National Research Council of Canada and the French Centre National de la Recherche Scientifique. The work is also based on observations obtained at the Gemini Observatory, which is operated by the Association of Universities for Research in Astronomy, Inc., under a cooperative agreement with the US NSF on behalf of the Gemini partnership: the US NSF, the STFC (United Kingdom), the National Research Council (Canada), CONICYT (Chile), the Australian Research Council (Australia), CNPq (Brazil), and CONICET (Argentina). This research used observations from Gemini programme numbers GN-2005A-Q-11, GN-2005B-Q-7, GN-2006A-Q-7, GS-2005A-Q-11, GS-2005B-Q-6, and GS-2008B-Q-56. This research has made use of the NASA/IPAC Extragalactic Database (NED), which is operated by the Jet Propulsion Laboratory, California Institute of Technology, under contract with NASA, and of data provided by the Central Bureau for Astronomical Telegrams.

Funding for the DES projects has been provided by the US Department of Energy, the US NSF, the Ministry of Science and Education of Spain, the Science and Technology Facilities Council of the United Kingdom, the Higher Education Funding Council for England, the National Center for Supercomputing Applications at the University of Illinois at Urbana-Champaign, the Kavli Institute of Cosmological Physics at the University of Chicago, the Center for Cosmology and Astro-Particle Physics at the Ohio State University, the Mitchell Institute for Fundamental Physics and Astronomy at Texas A&M University, Financiadora de Estudos e Projetos, Fundacao Carlos Chagas Filho de Amparo á Pesquisa do Estado do Rio de Janeiro, Conselho Nacional de Desenvolvimento Científico e Tecnológico and the Ministério da Ciência, Tecnologia e Inovacao, the Deutsche Forschungsgemeinschaft, and the Collaborating Institutions in the Dark Energy Survey.

The DES data management system is supported by the US NSF under grant AST-1138766. The DES participants from Spanish institutions are partially supported by MINECO under grants AYA2012-39559, ESP2013-48274, FPA2013-47986, and Centro de Excelencia Severo Ochoa SEV-2012-0234. Research leading to these results has received funding from the European Research Council under the European Union's Seventh Framework Programme (FP7/2007-2013) including ERC grant agreements 240672, 291329, and 306478. This research uses resources of the National Energy Research Scientific Computing Center, a DOE Office of Science User Facility supported by the Office of Science of the U.S. Department of Energy under Contract No. DE-AC02-05CH11231.

DATA AVAILABILITY STATEMENTS

The majority of the data have been already published and can be found in Poznanski et al. (2009) (KAIT-P09), D'Andrea et al. (2010) (SDSS-SN), de Jaeger et al. (2017a) (HSC), de Jaeger et al. (2019) (KAIT-d19), and de Jaeger et al. (2020) (DES-SN). CSP-I and SNLS data will be shared on a reasonable request to the corresponding author.

REFERENCES

Abbott B. P. et al., 2017, Nature, 551, 85
Aihara H. et al., 2018, PASJ, 70, S4
Anand G. S., Rizzi L., Tully R. B., 2018, AJ, 156, 105
Anderson J. P. et al., 2014, ApJ, 786, 67
Astier P. et al., 2006, A&A, 447, 31
Barbon R., Ciatti F., Rosino L., 1979, A&A, 72, 287
Benedict G. F. et al., 2007, AJ, 133, 1810
Bennett C. L. et al., 2003, ApJS, 148, 1
Bernstein J. P. et al., 2012, ApJ, 753, 152
Bonvin V. et al., 2017, MNRAS, 465, 4914
Burns C. R. et al., 2018, ApJ, 869, 56
Cardona W., Kunz M., Pettorino V., 2017, J. Cosmol. Astropart. Phys., 3, 056
Carrick J., Turnbull S. J., Lavaux G., Hudson M. J., 2015, MNRAS, 450, 317
Casertano S. et al., 2016, ApJ, 825, 11
D'Andrea C. B. et al., 2010, ApJ, 708, 661
de Jaeger T. et al., 2015, ApJ, 815, 121
de Jaeger T. et al., 2017a, MNRAS, 472, 4233
de Jaeger T. et al., 2017b, ApJ, 835, 166
de Jaeger T. et al., 2018, MNRAS, 478, 3776
de Jaeger T. et al., 2019, MNRAS, 490, 2799
de Jaeger T., et al., 2020, MNRAS, 495, 4860
Dhawan S., Jha S. W., Leibundgut B., 2018, A&A, 609, A72

Elias J. H., Matthews K., Neugebauer G., Persson S. E., 1985, ApJ, 296, 379
Feeney S. M., Mortlock D. J., Dalmasso N., 2018, MNRAS, 476, 3861
Filippenko A. V., 1997, ARA&A, 35, 309
Filippenko A. V., 2000, in Holt S. S., Zhang W. W., eds, AIP Conf. Proc. Vol. 522, Cosmic Explosions. Am. Inst. Phys., New York. p. 123
Filippenko A. V., Li W. D., Treffers R. R., Modjaz M., 2001, in Paczynski B., Chen W.-P., Lemme C., eds, ASP Conf. Ser. Vol. 246, Small Telescope Astronomy on Global Scales. Astron. Soc. Pac., San Francisco, p. 121
Fixsen D. J. , Cheng E.S. , Gales J. M., Mather J. C., Shafer R. A., Wright E. L., 1996, ApJ, 473, 576
Folatelli G. et al., 2010, AJ, 139, 120
Follin B., Knox L., 2018, MNRAS, 477, 4534
Foreman-Mackey D., Hogg D. W., Lang D., Goodman J., 2013, PASP, 125, 306
Freedman W. L., Madore B. F., 2010, ARA&A, 48, 673
Freedman W. L. et al., 2001, ApJ, 553, 47
Freedman W. L. et al., 2019, ApJ, 882, 34
Frieman J. A. et al., 2008, AJ, 135, 338
Gal-Yam A., 2017, Handbook of Supernovae, Springer-Verlag, Berlin, p. 195
Galbany L. et al., 2016, AJ, 151, 33
Ganeshalingam M. et al., 2010, ApJS, 190, 418
Graur O., Bianco F. B., Modjaz M., Shivvers I., Filippenko A. V., Li W., Smith N., 2017, ApJ, 837, 121
Hamuy M., Pinto P. A., 2002, ApJ, 566, L63
Hamuy M., Phillips M. M., Wells L. A., Maza J., 1993, PASP, 105, 787
Hamuy M. et al., 2006, PASP, 118, 2
Howell D. A., 2011, Nature Commun., 2, 350
Hsiao E. Y., Conley A., Howell D. A., Sullivan M., Pritchet C. J., Carlberg R. J., Nugent P. E., Phillips M. M. et al., 2007, ApJ, 663, 1187
Huang C. D. et al., 2020, ApJ, 889, 5
Hubble E., 1929, Proc. Natl. Acad. Sci. India, 15, 168
Humphreys E. M. L., Reid M. J., Moran J. M., Greenhill L. J., Argon A. L., 2013, ApJ, 775, 13
Jaffe A. H., Ade P. A., Balbi A. et al., 2001, Phys. Rev. Lett., 86, 3475
Jang I. S., Lee M. G., 2017a, ApJ, 835, 28
Jang I. S., Lee M. G., 2017b, ApJ, 836, 74
Janka H.-T., 2001, A&A, 368, 527
Janka H.-T., Langanke K., Marek A., Martínez-Pinedo G., Müller B., 2007, Phys. Rep., 442, 38
Kanbur S. M., Ngeow C., Nikolaev S., Tanvir N. R., Hendry M. A., 2003, A&A, 411, 361
Kim A., Goobar A., Perlmutter S., 1996, PASP, 108, 190
Kirshner R. P., Kwan J., 1974, ApJ, 193, 27
Kourkchi E., Tully R. B., Anand G. S., Courtois H. M., Dupuy A., Neill J. D., Rizzi L., Seibert M., 2020, ApJ, 896, 58
Lemaître G., 1927, Ann. Soc. Sci. Brux., 47, 49
Leonard D. C. et al., 2002, AJ, 124, 2490
Leonard D. C., Kanbur S. M., Ngeow C. C., Tanvir N. R., 2003, ApJ, 594, 247
Li W. et al., 2011, MNRAS, 412, 1441
Macaulay E. et al., 2019, MNRAS, 486, 2184
McQuinn K. B. W., Skillman E. D., Dolphin A. E., Berg D., Kennicutt R., 2017, AJ, 154, 51
Madore B. F., Mager V., Freedman W. L., 2009, ApJ, 690, 389
Minkowski R., 1941, PASP, 53, 224
Miyazaki S. et al., 2012, Proc. SPIE Conf. Ser. Vol. 8446, Ground-Based and Airborne Instrumentation for Astronomy IV. SPIE, Bellingham, p. 84460Z
Nugent P., Hamuy M., 2017, Handbook of Supernovae, Springer-Verlag, Berlin, p. 2671
Nugent P., Kim A., Perlmutter S., 2002, PASP, 114, 803
Oke J. B., Sandage A., 1968, ApJ, 154, 21
Olivares E F. et al., 2010, ApJ, 715, 833
Pastorello A. et al., 2006, MNRAS, 370, 1752
Perrett K. et al., 2010, AJ, 140, 518
Pesce D. W. et al., 2020, ApJ, 891, L1
Pietrzyński G. et al., 2013, Nature, 495, 76
Pietrzyński G. et al., 2019, Nature, 567, 200
Planck Collaboration et al., 2018, preprint (arXiv:1807.06209)
Poznanski D. et al., 2009, ApJ, 694, 1067
Poznanski D., Nugent P. E., Filippenko A. V., 2010, ApJ, 721, 956
Reid M. J., Pesce D. W., Riess A. G., 2019, ApJ, 886, L27
Riess A. G., 2020, Nature Rev. Phys., 2, 10
Riess A. G. et al., 2007, ApJ, 659, 98
Riess A. G. et al., 2009, ApJ, 699, 539
Riess A. G. et al., 2011, ApJ, 730, 119
Riess A. G., Casertano S., Anderson J., MacKenty J., Filippenko A. V., 2014, ApJ, 785, 161
Riess A. G. et al., 2016, ApJ, 826, 56
Riess A. G. et al., 2018a, ApJ, 855, 136
Riess A. G. et al., 2018b, ApJ, 861, 126
Riess A. G., Casertano S., Yuan W., Macri L. M., Scolnic D., 2019, ApJ, 876, 85
Rizzi L., Tully R. B., Makarov D., Makarova L., Dolphin A. E., Sakai S., Shaya E. J., 2007, ApJ, 661, 815
Rodríguez Ó., Clocchiatti A., Hamuy M., 2014, AJ, 148, 107
Rodríguez Ó. et al., 2019, MNRAS, 483, 5459
Sandage A., Tammann G. A., Saha A., Reindl B., Macchetto F. D., Panagia N., 2006, ApJ, 653, 843
Schlafly E. F., Finkbeiner D. P., 2011, ApJ, 737, 103
Schmidt B. P., Kirshner R. P., Eastman R. G., Phillips M. M., Suntzeff N. B., Hamuy M., Maza H., Aviles R., 1994, ApJ, 432, 42
Spergel D. N. et al., 2007, ApJS, 170, 377
Stahl B. E. et al., 2019, MNRAS, 490, 3882
Stritzinger M. et al., 2002, AJ, 124, 2100
Takáts K. et al., 2015, MNRAS, 450, 3137
Tully R. B., Fisher J. R., 1988, Catalog of Nearby Galaxies, Cambridge Univ. Press, Cambridge
Van Dyk S. D. et al., 2012, AJ, 143, 19
Vasylyev S. S., Filippenko A. V., 2020, ApJ, submitted
Wong K. C. et al., 2019, MNRAS, preprint (arXiv:1907.04869)
Woosley S. E., Weaver T. A., 1995, ApJS, 101, 181
Yuan W., Riess A. G., Macri L. M., Casertano S., Scolnic D. M., 2019, ApJ, 886, 61
Zgirski B. et al., 2017, ApJ, 847, 88
Zhang B. R., Childress M. J., Davis T. M., Karpenka N. V., Lidman C., Schmidt B. P., Smith M., 2017, MNRAS, 471, 2254

This paper has been typeset from a TEX/LATEX file prepared by the author.